The methyltransferase enzymes KMT2D, SETD1B, and ASH1L are key mediators of both metabolic and epigenetic changes during cellular senescence

Timothy Nacarelli[a], Ashley Azar[b], Manali Potnis[c], Gregg Johannes[d], Joshua Mell[e], F. Brad Johnson[f], Holly Brown-Borg[g], Eishi Noguchi[c], and Christian Sell[c,*]

[a]Glaxosmithkline, Oncology Synthetic Lethal Research Unit, Collegeville, PA 19426; [b]Merck, West Point, PA 19486; [c]Department of Biochemistry and Molecular Biology, Drexel University College of Medicine, Philadelphia, PA 19102; [d]Absorption Systems LLC, Exton, PA 19341; [e]Department of Microbiology and Immunology, Drexel University College of Medicine, Philadelphia, PA 19129; [f]Department of Pathology, University of Pennsylvania, Philadelphia, PA 19104; [g]Department of Biomedical Sciences, University of North Dakota School of Medicine and Health Sciences, Grand Forks, ND 58203

ABSTRACT **Cellular senescence is a terminal cell fate characterized by growth arrest and a metabolically active state characterized by high glycolytic activity. Human fibroblasts were placed in a unique metabolic state using a combination of methionine restriction (MetR) and rapamycin (Rapa). This combination induced a metabolic reprogramming that prevented the glycolytic shift associated with senescence. Surprisingly, cells treated in this manner did not undergo senescence but continued to divide at a slow rate even at high passage, in contrast with either Rapa treatment or MetR, both of which extended life span but eventually resulted in growth arrest. Transcriptome-wide analysis revealed a coordinated regulation of metabolic enzymes related to one-carbon metabolism including three methyltransferase enzymes (KMT2D, SETD1B, and ASH1L), key enzymes for both carnitine synthesis and histone modification. These enzymes appear to be involved in both the metabolic phenotype of senescent cells and the chromatin changes required for establishing the senescence arrest. Targeting one of these enzymes, ASH1L, produced both a glycolytic shift and senescence, providing proof of concept. These findings reveal a mechanistic link between a major metabolic hallmark of senescence and nuclear events required for senescence.**

Monitoring Editor
Coleen Murphy
Princeton University

Received: Aug 14, 2020
Revised: Feb 8, 2022
Accepted: Feb 17, 2022

This article was published online ahead of print in MBoC in Press (http://www.molbiolcell.org/cgi/doi/10.1091/mbc.E20-08-0523) on February 23, 2022.

Conflict of interest: The authors have no conflict of interest to declare in relation to the work presented in this manuscript.

Author contributions: T.N. performed the life span studies, respiration measurements, autophagy analyses, and helped to prepare the manuscript; A.A. carried out RNA sequencing and NanoString analyses, assisted with cell culture, immunoblotting experiments, and participated in preparation of the manuscript; J.M. assisted with RNA sequencing analyses; M.B. carried out nucleotide supplementation growth assays; G.J. assisted with experiments examining translational regulation and GCN2 activation; F.B.J. assisted with TIF analysis, provided conceptual input for experimental design and approaches, and assisted with the preparation of the manuscript; H.B-B. provided conceptual input for experimental design and assisted with the preparation of the manuscript; M. P. performed ATAC seq experiments and provided assistance with NanoString RNA analysis; C.S. provided conceptual input, carried out ASH1L knockdown and histone modification arrays, and assisted with preparation of the manuscript.

*Address correspondence to: Christian Sell (cs389@drexel.edu).

Abbreviations used: ATF4, activating transcription factor 4; ATG5, autophagy-related 5; BHMT, betaine-homocysteine S-methyltransferase; BWA, Burrows-Wheeler Aligner algorithm; CHOP, C/EBP homologous protein; CLPP, caseinolytic mitochondrial matrix peptidase proteolytic subunit; cPDL, cumulative number of population doubling; CTH, cystathionine gamma-lyase; CTP1, carnitine palmitoyltransferase 1; DAVID, Database for Annotation, Visualization and Integrated Discovery; ECAR, extracellular acidification rate; FCCP, carbonil-cyanide p-triflouromethoxyphenylhydrazone; GCN2, general control nonderepressible 2; GFP, green fluorescent protein; HCF, human cardiac fibroblast; KEGG, Kyoto Encyclopedia of Genes and Genomes; KMT2D, lysine-specific methyltransferase 2D; L2FC, log2-fold change; LC3B, light chain 3 beta; MetDEF, methionine deficient; MetR, methionine restriction; OCR, oxygen consumption rate; PCA, principle component analysis; qPCR, quantitative PCR; qRT-PCR, quantitative real-time PCR; Rapa, rapamycin; RPKM, reads per kilobase of transcript per million mapped reads; SASP, senescence-associated secretory phenotype; SDM, sample distance matrix; SETD1B, set domain-containing protein 1B.

INTRODUCTION

Human somatic cells have a finite life span in cell culture that is defined by the number of cell divisions that the population undergoes (Hayflick, 1965). Increasing DNA damage, ROS production, and mitochondrial dysfunction lead to the activation of stress response pathways, including the p53 and pRB pathways, to produce a terminal senescence arrest known as cellular or replicative senescence (Campisi, 2013). Although the senescence program has classically been described as a downstream consequence of DNA damage, it is becoming clear that metabolic disturbances can also trigger senescence (Berger and Sassone-Corsi, 2016; Nacarelli and Sell, 2016), and that metabolic interventions can delay senescence. The metabolic state of senescent cells is highly glycolytic, potentially due to the enhanced secretion of cytokines and proteolytic enzymes known as the senescence-associated secretory phenotype (SASP) (Bittles and Harper, 1984; James *et al.*, 2015; Wiley and Campisi, 2016). However, the altered metabolism of senescent cells may also play a causal role in senescence. For example, one consequence of the shift in metabolism appears to be a reduced NAD/NADH ratio leading to induction of AMPK which can directly phosphorylate and activate p53 in addition to stabilizing p21 mRNA levels (Wiley and Campisi, 2016). Given the complex nature of the senescent arrest, additional connections between metabolism and the senescence program likely exist. In this context, it would be predicted that interventions that alleviate this glycolytic shift should inhibit senescence. Consistent with this concept, we and others have reported that treatment with rapamycin (Rapa) or methionine restriction (MetR) can delay senescence in human diploid fibroblasts (Lerner *et al.*, 2013a; Johnson and Johnson, 2014; Koziel *et al.*, 2014). It appears that Rapa treatment extends the cellular life span, at least in part by reducing mitochondrial stress and enhancing utilization of alternative carbon sources (Lerner *et al.*, 2013a; Wang *et al.*, 2017; Nacarelli *et al.*, 2018). Similarly, MetR has been reported to reduce mitochondrial respiration and shift metabolism toward fat utilization in mice and to reduce complex IV activity and mitochondrial protein expression in human diploid fibroblasts (Koziel *et al.*, 2014).

In this study, we show that the combination of MetR plus Rapa produces a unique metabolic state, reducing mitochondrial respiration and preventing the glycolytic shift associated with senescence. The consequence is a block to entry into the senescent state.

RESULTS

Combining Rapa treatment and MetR dramatically increases the life span of human cardiac fibroblast cells

For analysis of life span, we examined senescence in human cardiac fibroblast (HCF) cells. Cardiac fibroblasts are the most abundant cell type in the human heart responsible for the extracellular matrix that provides structural support to the heart, the secretion of growth factors and cytokines, and dynamic remodeling following injury (Souders *et al.*, 2009; Rog-Zielinska *et al.*, 2016). Cardiac fibrosis is a significant component of nearly all forms of heart disease making the cardiac fibroblast a potential therapeutic target for age-associated dysfunction (Travers *et al.*, 2016). HCFs were cultivated under strict culture conditions for life span evaluation (Cristofalo and Charpentier, 1980) modified to include reduced concentrations of methionine (MetR) both in the presence and the absence of 1 nM Rapa. Methionine was reduced from 30 to 3 mg/l or 1 mg/l in MethR cultures. Methionine-deficient cultures (MetDEF), in which no methionine was added to the medium, were also included in the analysis with and without 1 nM Rapa. Replicative life span, determined by direct calculation of the cumulative number of population doublings (cPDLs), was significantly increased relative to standard culture conditions for MetR, Rapa treatment, or a combination of the two (Figure 1). Cultures treated with Rapa alone achieved a cPDL of 78 compared with a cPDL of 54 for control cultures, consistent with our previously published results (Bitto *et al.*, 2010; Lerner *et al.*, 2013b) and studies examining the impact of MetR on cellular life span (Johnson and Johnson, 2014; Koziel *et al.*, 2014). Combining the two treatments, MetR and Rapa had several surprising effects. First, the cultures treated with the combination Rapa+MetR proliferated more rapidly than cultures exposed to MetR, which had an acute negative impact on growth (note the difference in the slope of the curves between the MetDEF and the MethR [1 mg/l] and control cells in Figure 1). In contrast, the cultures treated with the combination Rapa+MetR proliferated more rapidly. Note the difference between methionine-restricted cultures and methionine-restricted cultures treated with Rapa (yellow line versus blue triangles in Figure 1 and gray circles versus green line in Figure 1). In addition, the combination of methionine restriction at 1 mg/l and 1 nM Rapa treatment provided a dramatic increase in life span ($P = 0.023$) compared with either treatment alone. In fact, cells cultured under this combination did not senesce and continued to proliferate for up to 1 year, reaching a cPDL of 91. In addition, the growth phenotype of late passage cells grown in methionine-restricted conditions with Rapa differed from cultures grown under standard conditions. Typically, cultures that enter senescence show a gradual reduction in cell number due to losses during harvesting and reseeding (note the downward trend in control cultures at the end of life span in Figure 1). In contrast, methionine-restricted/Rapa-treated cultures were doubling at an extremely slow rate (less than one doubling every 14 d) but did not enter a growth-arrested state. Life span analysis was repeated three times with similar results (see additional growth curves in Supplemental Figure S1, A and B) with cultures grown under standard conditions undergoing senescence at 50–56 cPDLs, while methionine-restricted cultures exhibited up to a 14% increase or 5–8 additional cPDLs. Rapa treatment generated a larger increase of up to 27% or 10–15 cPDLs and the combination of MetR plus Rapa treatment showed the largest increase, up to 69%, which represents 39 cPDLs. These results suggest that Rapa and MetR act in a synergistic manner. Rapa alleviated the acute growth deficit induced by MetR, and cultures subjected to a combination of MetR plus Rapa treatment are able to bypass senescence. Whether the MetDEF cultures eventually would have reached a population doubling greater than cultures in which methionine is restricted is not clear. Since these cells doubled so slowly, the experiment was terminated at 47 wk by harvesting RNA for analysis. In either case, it is clear that MetR and Rapa individually had an acute negative impact on proliferation, while the combination provided sustained proliferation. The addition of Rapa to methionine-restricted cultures provided the most robust increase in life span.

MetR plus Rapa treatment impacts both cell cycle and senescence markers

To further understand the acute impact of MetR plus Rapa treatment on proliferation, we analyzed the cell cycle profile of cells in log phase under each of the conditions (Experimental Point 1 in Figure 1). MetR induced an accumulation of G2 cells in the G2/M phase (4N). In addition, methionine-restricted cultures contained a population of cells with greater than 4N DNA content, suggesting cells occasionally re-replicated their DNA without passing through mitosis (Supplemental Figure S2A). Interestingly, Rapa treatment of the methionine-restricted cultures increased the growth rate, eliminated the polyploid population, and decreased the percentage of cells in G2 from 31 to 19% (Supplemental Figure S2B). Thus, MetR induced

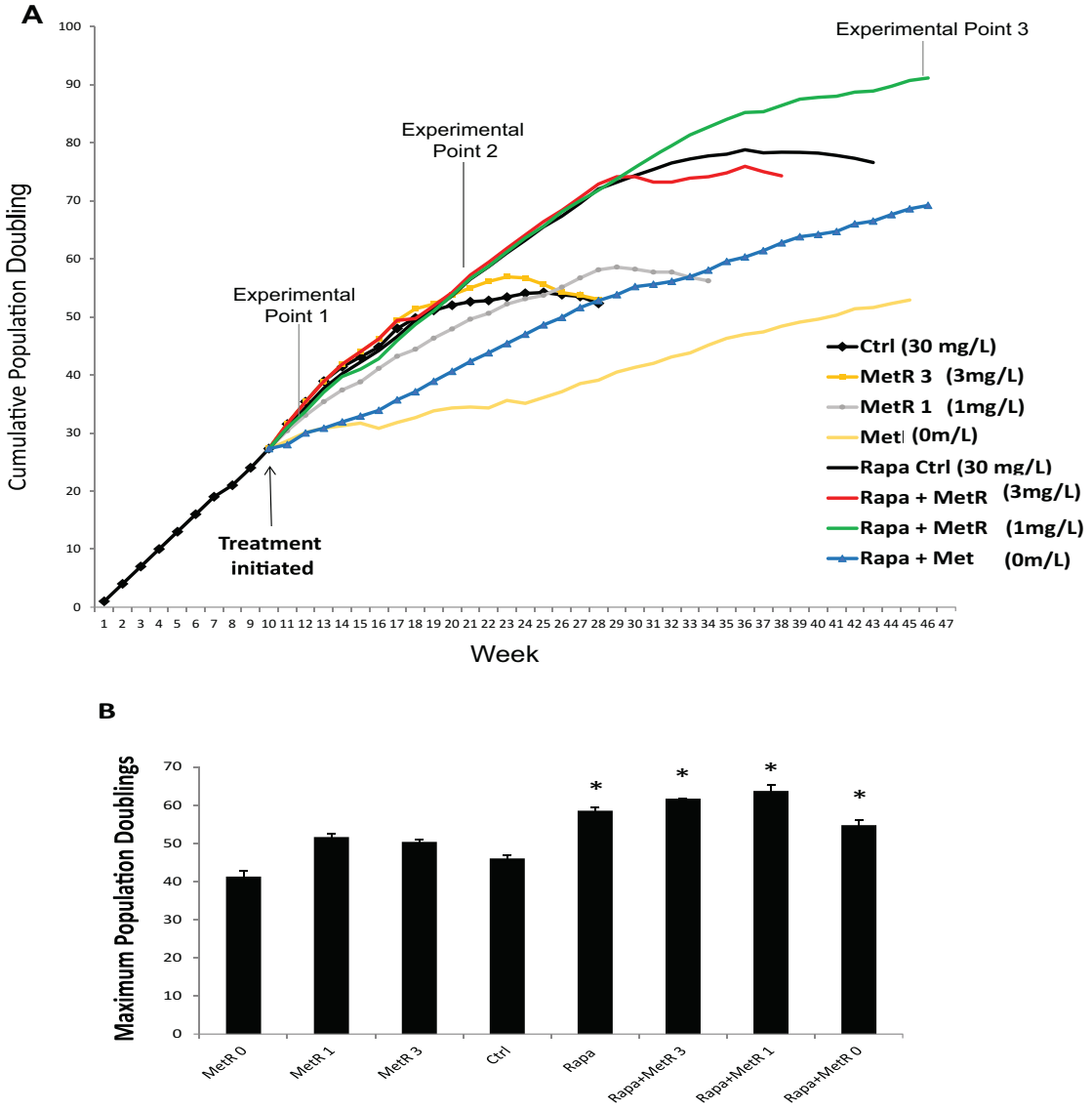

FIGURE 1: Combined MetR and Rapa treatment increases replicative life span in HCFs beyond MetR or Rapa alone. Panel (A) contains a representative life span analysis of HCFs maintained under the following conditions with or without 1 nM Rapa: standard culture conditions at 30 mg/l methionine (Ctrl), methionine-restricted at 3 mg/l methionine (MetR 3), methionine-restricted at 1 mg/l methionine (MetR 1), and methionine-deficient (MetDEF; no methionine added to the culture medium). Treatments were initiated at cumulative population doubling (cPDL) 27, as indicated by the arrow, using cultures maintained under control conditions from a cPDL of 3. Protein and/or RNA samples were collected at three points. Experimental Point 1 is the time when 50–60% of the life span is completed for the Ctrl cultures and all cultures have high proliferative potential. Experimental Point 2 is the time when 50–60% of the life span is completed for Rapa, MetR, and the combination Rapa+MetR. Ctrl cultures are entering senescence at this point. At Experimental Point 3, samples were taken from the combination Rapa+MetR for RNA sequence analysis. Life span analysis was performed three times with similar results and was performed at 6% oxygen with similar results. Panel (B) contains maximum life span as assessed by logistic regression analysis with 95% confidence intervals. In this graph. Conditions that show a significant difference ($P < 0.05$) from Ctrl for the average maximum cPDL were assessed from three independent experiments as assessed by T test are labeled with an asterisk. Growth rates at early passage of the MetR (0 mg/l and 1 mg/l) cultures were significantly reduced relative to Ctrl cultures (difference in growth rate over 5 wk, $P = 0.004$ for MetR 1 mg/l and $P = 0.002$ for MetR 0 mg/l, as assessed by two-tailed, unpaired T test), which revealed an acute negative impact on proliferation of these cultures. The addition of Rapa to these early passage cultures increased the growth rate such that there was no significant difference from controls. Life span curves were completed three times under ambient oxygen conditions and once in 5% oxygen. In all cases, the results were comparable. The combination of Rapa treatment and MetR increased life span beyond all other conditions and prevented senescence as judged by continued slow proliferation until termination of the experiment. In Panel (B), average data ± SD from three independent life span curves is presented. Maximum cPDLs were calculated using the logistic growth function in GraphPad to provide predicted maximal population doublings. Asterisks denote values that are statistically significant relative to control life span at $P < 0.05$.

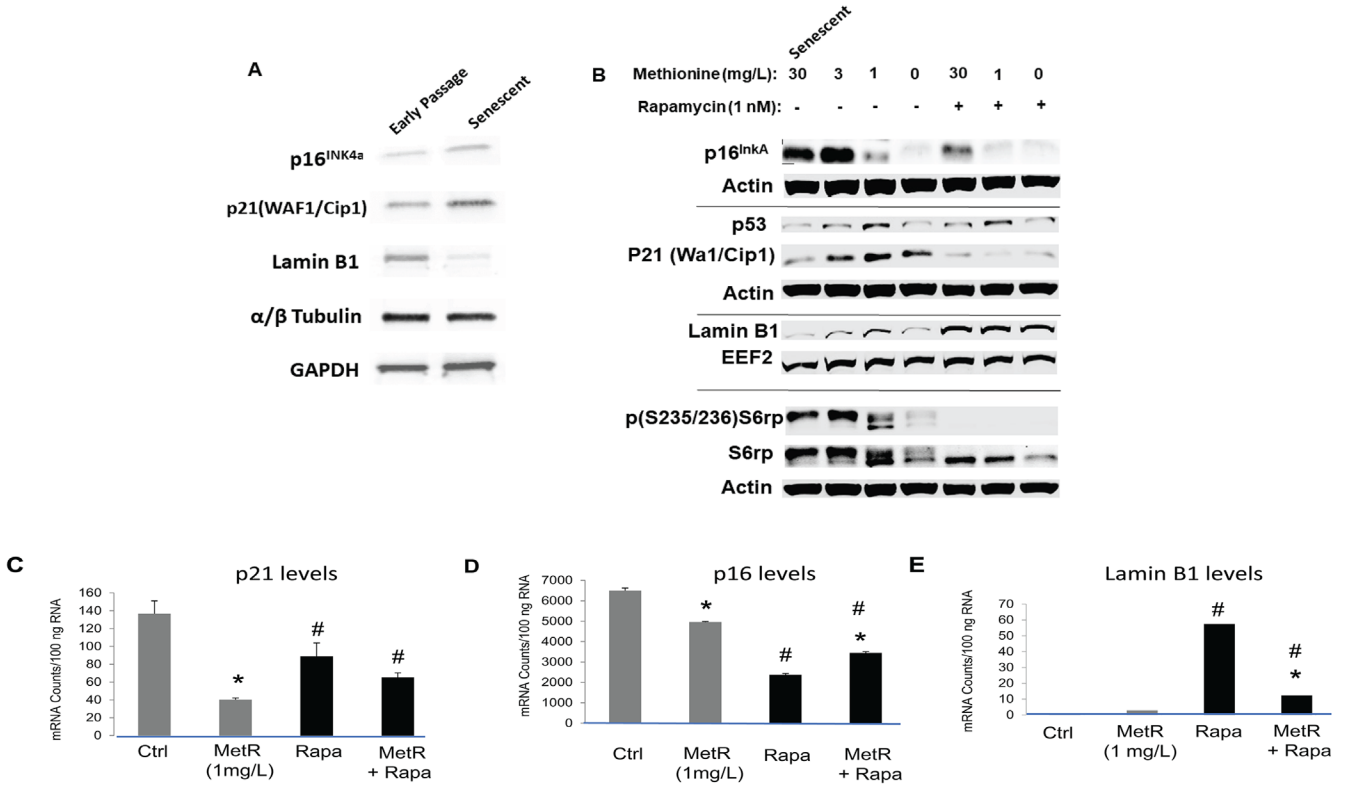

FIGURE 2: Markers of senescence are reduced with Rapa treatment and MetR. Steady-state protein (A, B) and mRNA (C–E) levels of senescence markers were examined by immunoblot and NanoString analysis, respectively. HCFs were grown under the indicated conditions and protein levels of p16, p53, p21, lamin B1, phosphorylated S6rp [p(S235/236)S6rp], and S6rp were determined by immunoblot analysis. Actin and EEF2 were used as loading controls. Panel (A) includes samples taken from early passage cultures compared with samples taken from senescent cells. The samples in (B) were taken at Experimental Point 2 in Figure 1. At this time, the control cultures (30 mg/l methionine without Rapa) were entering senescence and displaying characteristic changes in gene expression associated with senescence, such as increased $p16^{INK4A}$ and $p21^{Cip1/Waf1}$ levels and reduced lamin B1. A senescent cell sample is used as control for the data set in (B). The bar labels are as follows: standard conditions 30 mg/l methionine (Ctrl); 1 mg/l methionine (MetR); 1 nM Rapa treatment (Rapa); and a combination of MetR plus Rapa treatment (MetR + Rapa). Assessment of mRNA levels for $p21^{Cip1/Waf1}$ (C), $p16^{INK4A}$ (D), and lamin B1 (E) was performed at Week 4 of life span while protein levels were assessed at Week 23. Bars marked with an asterisk represent values that are significantly different from relative control values (without Rapa) at $P < 0.05$ and bars marked with a pound sign represent values that are significantly different between conditions with or without Rapa within the same methionine group (i.e., Ctrl, MetR) as evaluated using a two-tailed unpaired *T* test. Immunoblot analyses were repeated a minimum of three times and the Nanostring results are representative of two independent experiments. Nanostring results were verified by quantitative real-time RT-PCR.

a G2 block, consistent with previous reports (Yano *et al.*, 2014; Yano *et al.*, 2016), but this block was alleviated with the addition of Rapa.

We next sought to assess the impact of the various culture conditions on the senescence program. Senescence-associated molecular markers were examined at a point in the life span when the cultures under standard conditions exhibited a reduced proliferation rate and were nearing their maximal cPDL, i.e., the onset of senescence (Experimental Point 2 in Figure 1). At this point in their life span, control cells exhibited increased steady-state mRNA and protein levels of p21 and p16 (Figure 2, A–D). In contrast, the combination of MetR plus Rapa treatment reduced p16 protein and mRNA levels consistent with an inhibition of the senescence program (Figure 2B). MetR alone increased p21 protein levels, which is consistent with published results (Johnson and Johnson, 2014; Koziel *et al.*, 2014). However, the addition of Rapa to methionine-restricted cultures reduced p21 protein (Figure 2B), consistent with the cell cycle changes described in Supplemental Figure S2.

We also examined lamin B1 mRNA and protein levels because decreased expression of lamin B1 is a robust marker of senescence (Shimi *et al.*, 2011; Dreesen *et al.*, 2013; Shah *et al.*, 2013). The combination of MetR plus Rapa treatment preserved both lamin B1 protein and mRNA (Figure 2, A and E), although Rapa alone had the greatest impact on lamin B1 mRNA levels (Figure 2E). We also verified that Rapa suppressed mTORC1 signaling, as evidenced by a reduction in phosphorylation of the ribosomal S6 protein (Figure 2B). Interestingly, MetR also reduced S6 phosphorylation. Taken together, these results demonstrate that mTOR inhibition relieves the G2 block induced by MetR and that key mediators of the senescence program are not expressed in the presence of Rapa and MetR. Because telomere attrition plays an important role in replicative senescence, an analysis of telomere status in the cultures was performed. The cultures treated with the combination of MetR and Rapa at high population doublings had an average telomere length similar to the late passage HCF cells suggesting telomere attrition was not affected (Supplemental Figure S3A). In addition, telomerase

activity was undetectable in any of the cultures (Supplemental Figure S3B).

Methionine plus Rapa treatment enhances the rate of autophagy

Both Rapa treatment and MetR have been shown to activate autophagy, which is related to life span in yeast (Alvers *et al.*, 2009; Johnson and Johnson, 2014; Ruckenstuhl *et al.*, 2014), invertebrates (Hansen *et al.*, 2008; Bjedov *et al.*, 2010), and mammalian cells (Lerner *et al.*, 2013a; Liu *et al.*, 2015).To evaluate the impact of MetR plus Rapa treatment on autophagy in HCFs, we determined the autophagic flux in proliferating cultures (Experimental Point 1) based on 1) the turnover of both endogenous microtubule-associated protein 1 light chain 3 beta (LC3B) and green fluorescent protein (GFP)-tagged LC3B, 2) the presence of a cleavage product of GFP that is relatively stable in the lysosome, and 3) the number of LC3 puncta. By examining the relative levels of cytosolic LC3BI and autophagosome-associated LC3BII in the presence and absence of lysosomal inhibitors (leupeptin/NH_4), we can determine the flux of LC3B through the autophagy pathway. Immunoblots of endogenous LC3B are presented in Supplemental Figure S4A and the calculated rate of autophagic flux is presented in Supplemental Figure S4B.

Autophagic flux was significantly elevated by MetR and similarly by Rapa treatment, but the combination of the two conditions elevated flux to an even greater extent. We also determined the turnover of exogenous GFP-LC3B (Supplemental Figure S4C), which correlated with the turnover of endogenous LC3B. The cleavage product of the GFP protein was visualized following inhibition of lysosome activity (Supplemental Figure S4C); GFP-LC3B was used to visualize autophagosomes (LC3 puncta in Supplemental Figure S4, D and E) and provide a means to quantify the number of autophagosomes within a cell. Using this approach, we found that cells exposed to the combination of MetR plus Rapa treatment contained the highest number of autophagosomes (Supplemental Figure S4D). These results demonstrate that autophagy is elevated under conditions of MetR or Rapa treatment but is further enhanced when the two conditions are combined. To assess the potential impact of enhanced autophagy on cell function, we examined cell proliferation for up to 10 wk after targeting the autophagy-related 5 (ATG5) factor using an shRNA approach. Interestingly, we found that silencing ATG5 suppressed proliferation in cells cultured under standard conditions, while cultures grown under all other conditions continued to proliferate, suggesting that both MetR and Rapa treatment create a setting in which cells are able to compensate for reduced ATG5 levels and maintain proliferation (Supplemental Figure S4F).

We next explored the mechanisms leading to the enhanced autophagy induced by the combination of MetR plus Rapa treatment. Two major nutrient sensors that regulate autophagy are mTORC1 and general control nonderepressible 2 (GCN2). Phosphorylation of GCN2 and the ternary complex protein eIF2α increased in cultures subjected to MetR plus Rapa treatment compared with either treatment alone (Supplemental Figure S5A). Consistent with increased GCN2 activity, activating transcription factor 4 (ATF4), C/EBP homologous protein (CHOP), and caseinolytic mitochondrial matrix peptidase proteolytic subunit (CLPP) mRNA levels were also elevated (Supplemental Figure S5B). We also found that the combination of MetR plus Rapa treatment elevated ATG12 and ATG5 protein levels (Supplemental Figure S5A). These results reveal a synergistic effect of Rapa treatment and MetR on both GCN2 signaling and the rate of autophagy, both of which are known to increase stress resistance.

Transcriptome-wide analysis reveals that methionine-restricted cultures treated with Rapa do not produce a senescent profile at high population doublings

To understand how the MetR plus Rapa-treated cells may be able to evade senescence, we turned to a global assessment of the impact of MetR plus Rapa treatment using RNA sequencing analysis. RNA was isolated from both early passage cells at cPDL 30, which represents the point at which 50–60% of the life span is completed for these cultures (Experimental Point 1 in Figure 1) and late passage cells at cPDL 52 (Experimental Point 2 in Figure 1) when the cultures were entering senescence. RNA was isolated from methionine-restricted, Rapa-treated, and combination methionine-restricted/Rapa-treated cells at Week 20 (Experimental Point 2 in Figure 1). This is a point at which the treated cells retain high proliferative capacity and were surpassing the maximal life span of control cultures. It represents 50–60% life span completion for these cultures. RNA was also isolated at Week 47 (Experimental Point 3 in Figure 1) from the MetR plus Rapa-treated cells to determine whether these cells eventually express a senescent transcriptome profile. Prior to differential expression analyses, RNA sequence data were subjected to a series of validation analyses including internal validation between sequencing runs and a comparison to a custom Nanostring gene panel which included senescence-related genes. RNA sequencing was performed in triplicate with the exception of the very late passage (cPDL91, Experimental Point 3 in Figure 1) cultures exposed to MetR plus Rapa treatment, which were run in duplicate due to the limited amount of material.

Next, we confirmed that RNA isolated from the untreated late passage cells displayed a gene expression profile consistent with senescence by examining the expected increase in mRNA levels of CDKN1A, CDKN2A, IL6, IGF1R, IGFBP5, and IGFBP7, as well a decrease in LMNB1 mRNA, which is known to occur during senescence (Shimi *et al.*, 2011). Volcano plots of differentially expressed genes between early and late passage, as well as a comparison of early passage to the very late passage MethR plus Rapa treatment, are presented in Figure 3, A and B. Evaluation of a subset of gene expression changes known to occur with senescence (Coppe *et al.*, 2008; Coppe *et al.*, 2010) in both settings reveals that the control cultures display a pattern consistent with senescence while these genes show a very different pattern of expression in the very late passage MethR plus Rapa cultures (bar graphs in Figure 3, A and B). Similarly, an evaluation of genes associated with the proinflammatory phenotype of senescent cells, the SASP, revealed a differential impact of the treatments. A subset of SASP factors, such as IL-6, were reduced most strongly by Rapa, while others, such as IGFBP3 were more strongly affected by MtheR (Supplemental Figure 6). Given the remarkable longevity of the cultures exposed to the combined MetR plus Rapa treatment, we sought to determine whether these cells eventually activate the senescence program using a global approach. We expanded the transcriptome comparison to produce a sample distance matrix (SDM) based on the overall similarity of gene count profiles between each sample and calculated Euclidean distances within DESeq2 (Figure 3C). The differences in sample distance can be appreciated in the SDM in Figure 3C by examining the numerical values and shading. The values correlate with the intensity of shading where darker blue indicates a greater similarity or smaller Euclidean distance. Numerical values are inversely related to distance. The greatest similarity is found on the diagonal, as samples are most highly related to themselves with values of 0. Samples within replicates fall within a Euclidean distance of approximately 30–50, whereas more distantly related samples produce a Euclidean distance of 150 or greater. At cPDL 91,

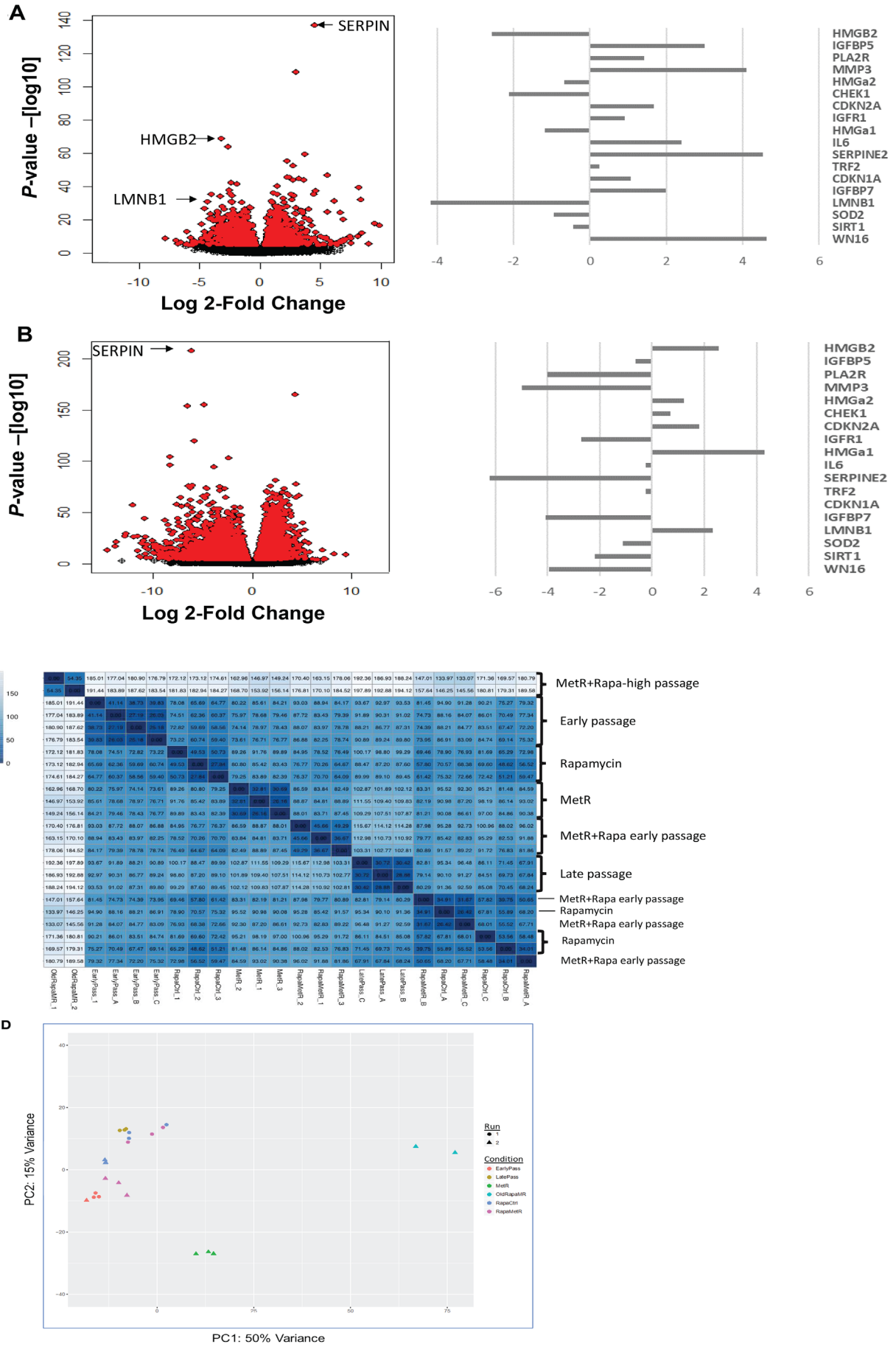
A
P-value –[log10]
SERPIN
HMGB2
LMNB1
Log 2-Fold Change
HMGB2
IGFBP5
PLA2R
MMP3
HMGa2
CHEK1
CDKN2A
IGFR1
HMGa1
IL6
SERPINE2
TRF2
CDKN1A
IGFBP7
LMNB1
SOD2
SIRT1
WN16
B
P-value –[log10]
SERPIN
Log 2-Fold Change
HMGB2
IGFBP5
PLA2R
MMP3
HMGa2
CHEK1
CDKN2A
IGFR1
HMGa1
IL6
SERPINE2
TRF2
CDKN1A
IGFBP7
LMNB1
SOD2
SIRT1
WN16
C
MetR+Rapa-high passage
Early passage
Rapamycin
MetR
MetR+Rapa early passage
Late passage
MetR+Rapa early passage
Rapamycin
MetR+Rapa early passage
Rapamycin
MetR+Rapa early passage
D
PC2: 15% Variance
PC1: 50% Variance
Run
Condition
EarlyPass
LatePass
MetR
OldRapaMR
RapaCtrl
RapaMetR

cultures exposed to both MetR plus Rapa treatment exhibited a Euclidean distance of greater than 180 to both early passage and late passage control cultures, indicating little similarity to either state. These results suggest that although the growth rate is significantly reduced at early passage by MetR plus Rapa treatment, the senescence program is not activated under these conditions. Additionally, a principle component analysis (PCA) was conducted to further distinguish the relative similarity of samples in our study. This PCA was able to model approximately 50% of the variability in our data. In the PCA plot in Figure 3D, the late passage samples group separated from the early passage samples. The Rapa-treated cells and the combination-treated cells cluster between the early and the late passage cells. Interestingly, we observed distinct clustering of MetR cells and a more distant cluster containing the very late passage combination MetR plus Rapa cells, confirming the SDM analysis which indicated that the very late passage combination MetR plus Rapa-treated cultures have a unique transcriptional profile not related to senescence.

As an independent verification that the MetR/Rapa cells do not senesce, we examined the chromatin state using ATAC seq. In this approach, areas of euchromatin and heterochromatin can be evaluated. Senescent cells are known to undergo chromatin remodeling at multiple levels from nucleosome density to higher-order structural changes (Parry and Narita, 2016). Genomewide overviews of the ATAC seq data reveal a distinct expansion of heterochromatic regions in senescent cells consistent with the epigenetic modifications associated with senescence. The expansion of these regions is not apparent in late passage cells treated with the MetR plus Rapa combination (see chromosome 9 presented in Figure 4A and each individual chromosome presented in Supplemental File 2). These areas generally correlate with regions lacking H3K27 acetylation and relative inaccessibility to DNAse cleavage (see UCSC tracks included in Figure 4A). Published data using FAIRE analysis indicate a general silencing of promoter elements during senescence coupled with enhanced signal from heterochromatic regions (De Cecco *et al.*, 2013). Global analysis of the ATAC sequencing analysis reflects this shift with a reduced accessibility of promoter regions coupled with increased accessibility in intergenic regions (Figure 4B), suggesting that we are able to visualize the expected changes associated with senescence in the analysis. Interestingly, a reduction in peak density in exons is observed in senescent cells and this shift appears to also occur in the late passage MetR plus Rapa combination (Figure 4B). Additional RNA-Seq analysis was performed to understand the unique gene expression profile of the combination-treated cells when they reach an extended life span (Week 47). In this analysis, the MetR plus Rapa cultures at very late passage were compared with every other treatment in the study and a list of differentially expressed genes was established using DESeq2. With a threshold of an absolute value log2-fold change (L2FC) of 2.5, we identified 1756 differentially expressed genes: 266 genes were up-regulated and 1490 genes were down-regulated. A Database for Annotation, Visualization and Integrated Discovery (DAVID) pathway analysis was performed and 10 pathways were identified that were potentially activated based on the analysis of up-regulated genes. DAVID pathway analysis also identified 57 pathways that were potentially repressed based on the down-regulated genes. To narrow down the affected pathways based on down-regulated genes, only the top 250 genes were used in the pathway analysis. The gene lists were used for comparisons between groups as outlined in Supplemental Figure S7 in diagram form; 12 pathways were detected. The most significant positively affected pathway was the ribosome synthesis pathway. Interestingly, the list of genes included genes encoding both nuclear and mitochondrial ribosomal proteins, suggesting an impact on both cytoplasmic and mitochondrial protein synthesis. Additional up-regulated pathways included pyrimidine metabolism, vascular smooth muscle contraction, oocyte meiosis, cell cycle, progesterone-mediated oocyte maturation, purine metabolism, oxidative phosphorylation, VEGF signaling, and MAPK signaling. The

FIGURE 3: HCFs exposed to MetR plus Rapa treatment do not undergo replicative senescence. Panel (A) contains a volcano plot showing differential gene expression analysis of late passage control cells compared with early-passage control cultures. The graph compares the log [2-fold change] in sequencing counts with the (–)log 10 of the *P* value for each comparison. A total of 789 mRNA sequences met the criteria of $P < 0.05$ and a log 2-fold change of 2. A subset of genes whose expression levels are known to be altered during the senescence program were identified in the analysis and these genes are presented in the bar graph to the right of the plot. Three senescence-related genes from this list are labeled in the volcano plot. Panel (B) contains an identical comparison as in (A) comparing early passage cells with the very late-passage MethR + Rapa-treated cells at PD 91. Note that the senescence-associated genes show a completely different pattern of expression from the results in (A). Panel (C) contains the results of distance matrix analysis for all cultures in the study. Early passage cells were used at Week 4, while late passage, Rapa-treated, MetR, and Rapa+MetR were used at Week 23 (Experimental Points 1 and 2 in Figure 1). Samples labeled EarlyPass represent values from early passage (cPDL 25) cells. Samples labeled RapaCtrl contain values from cultures treated with only Rapa. Samples labeled MetR contain values from methionine-restricted (1 mg/l) cultures. Samples labeled RapaMetR contain values from cultures exposed to MetR plus Rapa. Samples labeled LatePass contain values from senescent control cultures. The Rapa+MetR samples were used at Week 47 (Experimental Point 3 in Figure 1). These late passage (cPDL 91) cultures maintained under the combination of MetR plus Rapa treatment are labeled OldRapaMR. The gene count profile from each RNA-Seq sample was compared with all other RNA-Seq samples to evaluate general similarity. Darker blue shading indicates a shorter Euclidean distance (greater similarity) compared with lighter blue shading which indicates a longer distance. Each block contains the numerical Euclidean distance for the given comparison with a higher number indicating a greater distance. The diagonal shows zeros indicating that a sample compared with itself gives an identical value, as similarity between samples is inversely related to distance. Samples with names ending in a letter were included in RNA-Seq Run 1. Samples with names ending in a number were included in Run 2. Panel (C) contains the results of a PCA of the RNA-Seq data. The plot represents the general similarity of each sample based on the top 500 differentially expressed genes. Circles represent samples run in the first round of sequencing and triangles represent samples run in the second round of sequencing. Each treatment is color coded. Note that the samples from the very late passage MethR plus Rapa treatment cultures cluster separately from all other samples in accordance with the SDM results.

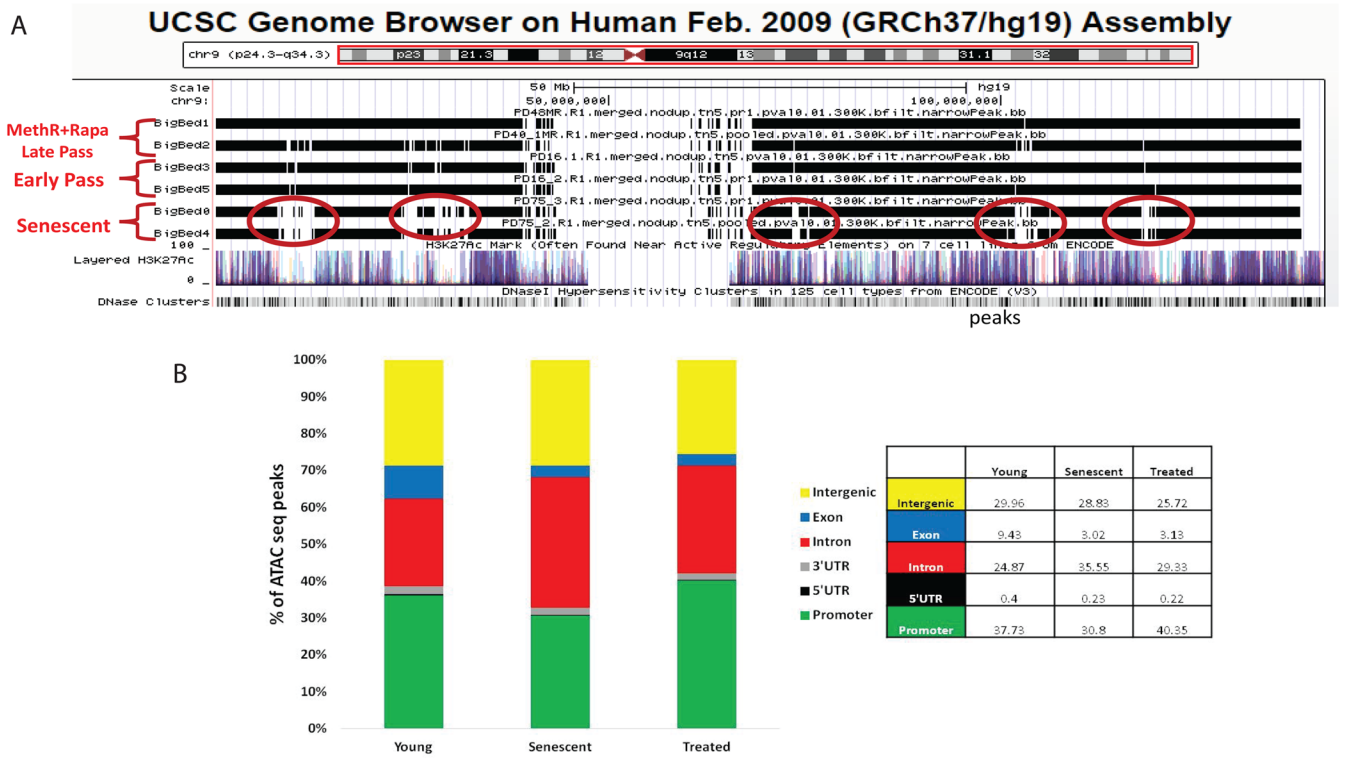

	Young	Senescent	Treated
Intergenic	29.96	28.83	25.72
Exon	9.43	3.02	3.13
Intron	24.87	35.55	29.33
5'UTR	0.4	0.23	0.22
Promoter	37.73	30.8	40.35

FIGURE 4: MetR plus Rapa treatment preserves chromatin accessibility. Panel (A) contains chromatin accessibility as assessed by ATAC seq analysis for a representative chromosome (chromosome 9). Two independent replicates from cultures at early passage, late passage (senescent), and late passage treated with MetR plus Rapa are presented. In (A), peaks are presented as black lines, resulting in dark regions denoting high accessibility, while regions of reduced accessibility lack coverage and appear as white areas (indicated by red circles on senescent tracks). For comparison, UCSC tracks denoting ENCODE generated open chromatin marks (DNAse hypersensitivity and Histone H2K27ac) are presented below the ATAC seq analysis. Panel (B) contains an analysis of the relative peak density in intergenic, intron, exon, 5′ UTR, and promoter regions in each sample set.

12 pathways that were down-regulated included renin secretion, cGMP-PKG signaling, ovarian steroidogenesis, calcium signaling, cAMP signaling, retinol metabolism, PI3K-Akt signaling, cancer pathways, cytokine–cytokine receptor interaction, Rap1 GTPase signaling, protein digestion and absorption, as well as pancreatic secretion. These results indicate that cultures maintained under conditions of MetR plus Rapa treatment at high population doublings have a unique expression profile that is not comparable to late passage cultures grown under standard culture conditions.

Next, we wanted to compare the MetR, Rapa, and combination cultures to identify genes expressed uniquely in cells exposed to the combination at midlife span, since these changes might enable the cultures to evade senescence. A list of genes, uniquely differentially expressed when ~50% of the life span was completed for the Rapa-treated, MetR cultures (Experimental Point 2) relative to control cultures when ~50% of the life span was completed (Experimental Point 1), is shown in Table 1. To generate the gene list in Table 1, differentially expressed genes with an L2FC and an adjusted P value < 0.05 were established ($P < 0.05$ and L2FC>|1|) for each condition (MetR, Rapa treatment, and combination MetR plus Rapa). Lists were compared with one another as shown in the Venn diagram in Supplemental Figure S7. Genes that were differentially expressed under the combination condition alone were considered uniquely expressed in the combination and subjected to DAVID Functional Annotation Analysis. No functional pathways were identified for genes with reduced expression. DAVID pathways identified as up-regulated and most related to nutrient sensing included lysine degradation, glycine, serine, threonine metabolism, and thyroid hormone signaling. Examining the genes identified by DAVID as belonging to these pathways revealed several genes related to methionine metabolism in each pathway. For example, the differential expression of genes related to the recycling of methionine from homocysteine was the basis for the identification of the glycine, serine, and threonine metabolism pathways. These genes included betaine-homocysteine S-methyltransferase (BHMT), which catalyzes the synthesis of methionine using homocysteine and the methyl donor betaine and cystathionine gamma-lyase (CTH), also involved in homocysteine metabolism and the transsulfuration pathway, which is required for longevity in response to dietary restriction (Pajares and Perez-Sala, 2006; Kabil *et al.*, 2011). The thyroid hormone signaling pathway was identified by the differential expression of seven genes including 6-phosphofructo-2-kinase/fructose-2,6-biphosphatase 2, a critical regulator of glycolysis. Finally, differentially expressed genes in the lysine degradation pathway included ASH1L, set domain-containing protein 1B (SETD1B), and lysine-specific methyltransferase 2D (KMT2D), which were significantly increased in cultures exposed to the combination of MetR plus Rapa treatment. These enzymes act in concert to produce trimethyllysine, the first step in a direct pathway to produce carnitine. Carnitine is an indispensable mediator of intermediary metabolism required for transporting long chain acyl groups across the mitochondrial membrane by carnitine palmitoyltransferase 1 (CPT1) to facilitate beta oxidation (Britton *et al.*, 1995; Bonnefont *et al.*, 2004; Strijbis *et al.*, 2010). In our transcriptome analysis, CPT1 was also increased significantly under the combined conditions of MetR

KEGG pathway (unique to combo)	No. genes	Gene names	*P* value	Adjusted *P* value
Glycine, serine, threonine metabolism	5	BHMT, CTH, DMGDH, GLDC, PSAT1	3.2×10^{-3}	0.28
Axon guidance	8	EPHA4, ROCK2, NTN2, PAK2, PLXNA2, PPP3R1, SEMA3C, UNC5B	3.8×10^{-3}	0.42
Thyroid hormone signaling	7	PFKB2, MDM2, MED13L, NOTCH1, NOTCH2, THRB, MYC	9×10^{-3}	0.40
Taste transduction	4	SCNN1A, TAS1R3, TAS2R31, TAS2R5	3.4×10^{-2}	0.71
Lysine degradation	4	ASH1L, SETD1B, KMT2D, COLGALT2	4.8×10^{-2}	0.8
T cell receptor signaling pathway	5	FOS, PAK2, PPP3R1, PTPRC, TEC	7.9×10^{-2}	0.9
Proteoglycans cancer	7	MDM2, ROCK2, TIAM1, ANK2, ERBB3, MYC, VEGFA	9.6×10^{-2}	0.91

TABLE 1: Gene pathways uniquely up-regulated in cultures maintained in metR + Rapa.

plus Rapa treatment in both early and late passage cells versus early passage controls (1.6- and 4-fold; adjusted $P = 0.0095$ and $P = 6.2 \times 10^{-4}$, respectively). These results indicate that the combination of mTOR inhibition and MetR induces a unique transcriptional profile that includes the expression of multiple enzymes involved in methionine metabolism, mitochondrial activity, and potentially, chromatin remodeling. Based on this analysis, we developed a working model in which MetR + Rapa induces the expression of KMT2D, SETD1B, and ASH1L to enhance beta oxidation and impact histone modifications leading to a block to senescence.

Cultures subjected to MetR plus Rapa are able to maintain oxidative phosphorylation and prevent the senescence-associated glycolytic shift

To verify that the differences in gene expression are reflected in functional differences at the cellular level, we sought to determine whether we could detect a difference in fatty acid oxidation as predicted by the increase in enzymes leading to carnitine production. Consistent with our previous work (Nacarelli *et al.*, 2018), the oxygen consumption rate (OCR) was increased in senescent cells. In addition, we examined respiration rates in cultures exposed to MetR, Rapa treatment, and the combination. In this assay, exogenous palmitate is added to cultures and the resultant change in oxygen consumption provides an indication of the relative ability of the culture to use beta oxidation. An initial analysis comparing early and late passage cells revealed that early passage cells increased their OCR when provided with exogenous palmitate, an effect that was blocked by etomoxir, an irreversible inhibitor of CPT1 (Figure 5A). In contrast, late passage cells were unable to increase their OCR when provided with exogenous palmitate, and etomoxir had little influence on the OCR. Rapa treatment allowed late passage cells to respond to palmitate in a manner similar to early passage cells (Figure 5B). MetR did not have a significant effect on response to palmitate but increased response to etomoxir. Cells exposed to the combination treatment exhibited the most robust response of all conditions tested (Figure 5C). In addition, glucose uptake was lowest in those cells subjected to the combination treatment (Figure 5D). In parallel with OCR, we were able to simultaneously measure the extracellular acidification rate (ECAR). The ECAR largely reflects the glycolytic rate, although other cellular processes can contribute to the ECAR. The ratio of oxygen consumption to extracellular acidification provides a measure of the relative use of oxidative phosphorylation versus glycolysis. Of the growth conditions tested, cells subjected to the combination MetR plus Rapa treatment exhibited a significantly lower basal respiration and ECAR. These cells also had a significantly increased metabolic ratio (OCR/ECAR), suggesting a greater dependence on mitochondrial oxidative phosphorylation over glycolysis, while senescent cells showed greater glucose utilization relative to all other conditions.

By examining the OCR of cells following the sequential addition of inhibitors of the mitochondrial pyruvate transporter (UK5099), glutaminase (BPTES), and CPT1 (etomoxir), one can assess the relative ability of the culture to alternate between carbon sources to maintain oxidative capacity. By subjecting cultures under the various growth conditions to this analysis, we found that cells maintained under a combination of MetR plus Rapa treatment exhibited a significantly increased capacity for alternating between pyruvate and glutamine/fatty acids to support oxygen consumption, compared with metR or Rapa treatment alone. Senescent cells exhibited the lowest capacity for alternating between carbon sources (Figure 6). These analyses suggest that cultures maintained under a combination of MetR plus Rapa treatment have an increased capacity for beta-oxidation and an enhanced ability to alternate between carbon sources consistent with the increased expression of CPT1, KM2D, SETD1B, and ASH1L.

Histone H3 levels are maintained by MetR plus Rapa while knockdown of ASH1L induces senescence

We next sought to confirm that the activity of the histone H3 methyltransferases KMT2D, ASH1L, and SET2D was essential for the maintenance of a proliferative phenotype in HCFs. We first confirmed the altered mRNA levels of these enzymes (Figure 7A) and introduced a set of five short hairpin (sh)RNA targeting vectors directed against ASH1L because this enzyme displayed the greatest elevation in mRNA levels and the target histone H2K36 is important for transcriptional fidelity (He *et al.*, 2008; Sen *et al.*, 2015). Of the five targeting vectors, two produced a significant decrease in ASH1L mRNA levels (Figure 7B). Cells harboring these vectors underwent senescence within 5 d of selection. These cultures acquired the classic senescent phenotype of enlarged cells that stain strongly for the senescence-associated β-galactosidase activity (Figure 7, C and D). These results confirm that expression of ASH1L is required to maintain the proliferative state and that decreased expression of ASH1L can trigger senescence. We also examined the potential consequences of MetR plus Rapa on histone H3 abundance, which is known to decrease during senescence (Ivanov *et al.*, 2013; Duarte *et al.*, 2014). Total levels of histone H3 were increased relative to late passage cells (Figure 7E) as were histone H3 modifications at H3K36 (Figure 7F). The metabolic consequences of targeting ASH1L were examined by evaluating ECARs in the presence and absence of mitochondrial inhibitors. ASH1L targeting resulted in a glycolytic shift consistent with induction of senescence (Figure 7, G and H).

DISCUSSION

We report the rather surprising result that normal diploid fibroblasts can evade the senescence program under the appropriate conditions. In examining the impact of two interventions known to

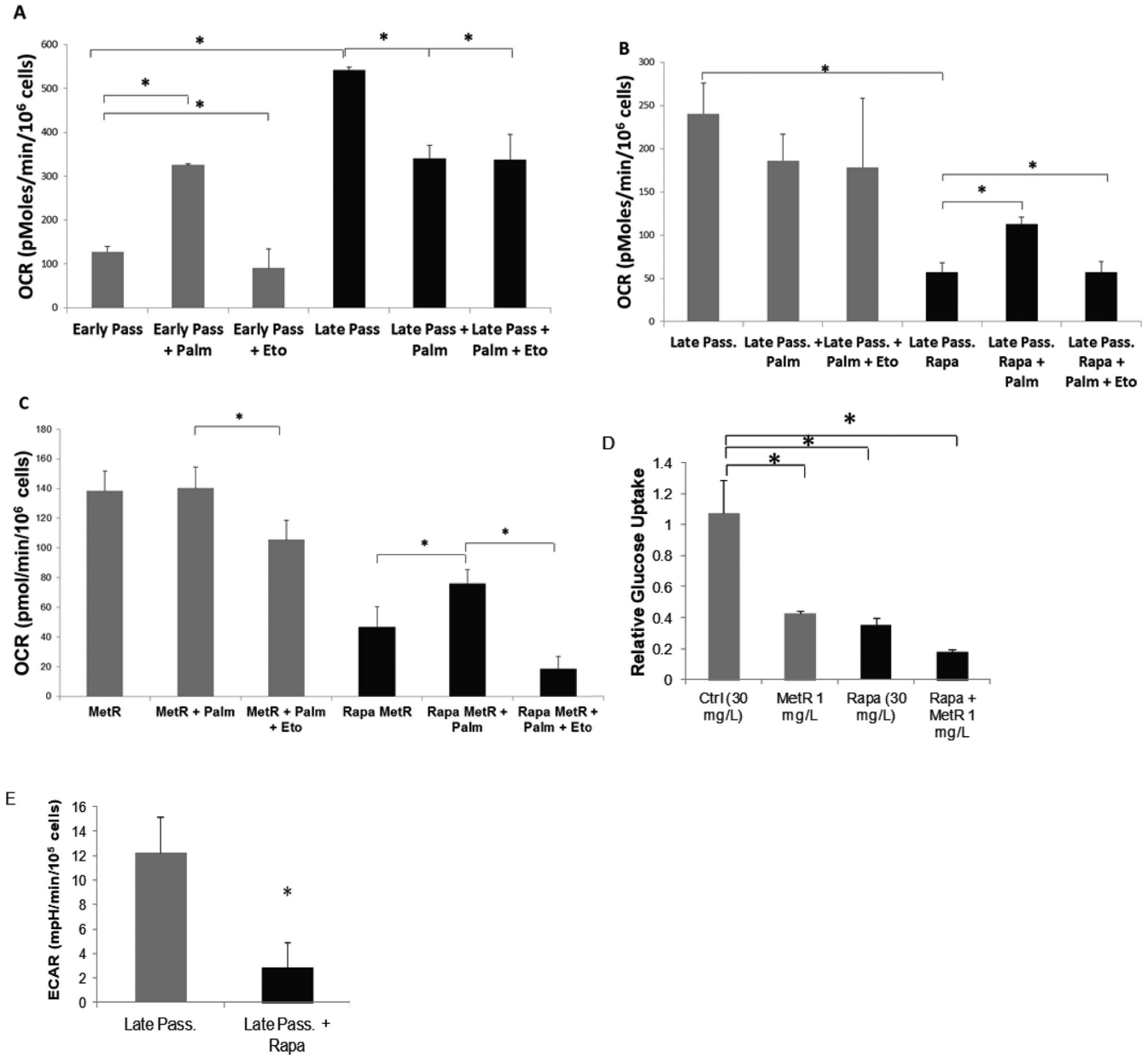

FIGURE 5: The combination of Rapa treatment plus MetR increases fatty acid utilization. Metabolic flexibility is defined as the ability to maintain oxygen consumption following treatment with metabolic pathway pharmacological inhibitor(s). Panel (A) compares the OCR in response to palmitate (palm) and an inhibitor of CPT1 (etomoxir [eto]) in early-passage versus late passage (senescent) cultures. Panel (B) shows results comparing late passage cultures versus late passage cultures treated with Rapa. Panel (C) shows the results of a comparison between methionine-restricted cultures and cultures subjected to the combination ofRapa plus MetR (1 mg/l) treatment. Panels (D) and (E) contain results of glucose utilization rates and ECARs, respectively. Results are representative of at least two independent experiments and significance ($P < 0.05$) in unpaired *T* tests between samples and is indicated by asterisks.

influence cellular metabolism, MetR and Rapa treatment, we noted several unexpected interactions. Both MetR and Rapa treatment are known to decrease the growth rate of human fibroblasts (Lerner *et al.*, 2013a; Johnson and Johnson, 2014; Koziel *et al.*, 2014). The anticipated outcome of combining these two treatments would be a further reduction in growth or perhaps cell death; however, we find the opposite. Rapa at nanomolar concentrations alleviates the G2 arrest and rescues the growth deficit associated with MetR. Detailed analysis of gene expression profiles and heterochromatin in these cultures confirms that the cells do not exhibit characteristics of senescence.

In terms of the mechanism by which MetR plus Rapa treatment enables the cells to evade senescence, mTOR is known to regulate glycolysis and has been implicated as a mediator of the Warburg effect in cancer (Yecies and Manning, 2011). Given that the mTOR pathway is active in both senescent cells and a variety of aging tissues (Nacarelli *et al.*, 2015), it seems clear that the glycolytic state of senescent cells is at least partially dependent on mTOR activity, and inhibition of mTOR signaling prevents the glycolytic shift. The unique aspect of the current study is that the rather extreme metabolic state induced by MetR in combination with inhibition of the mTOR pathway reveals metabolic responses that may not be easily detected

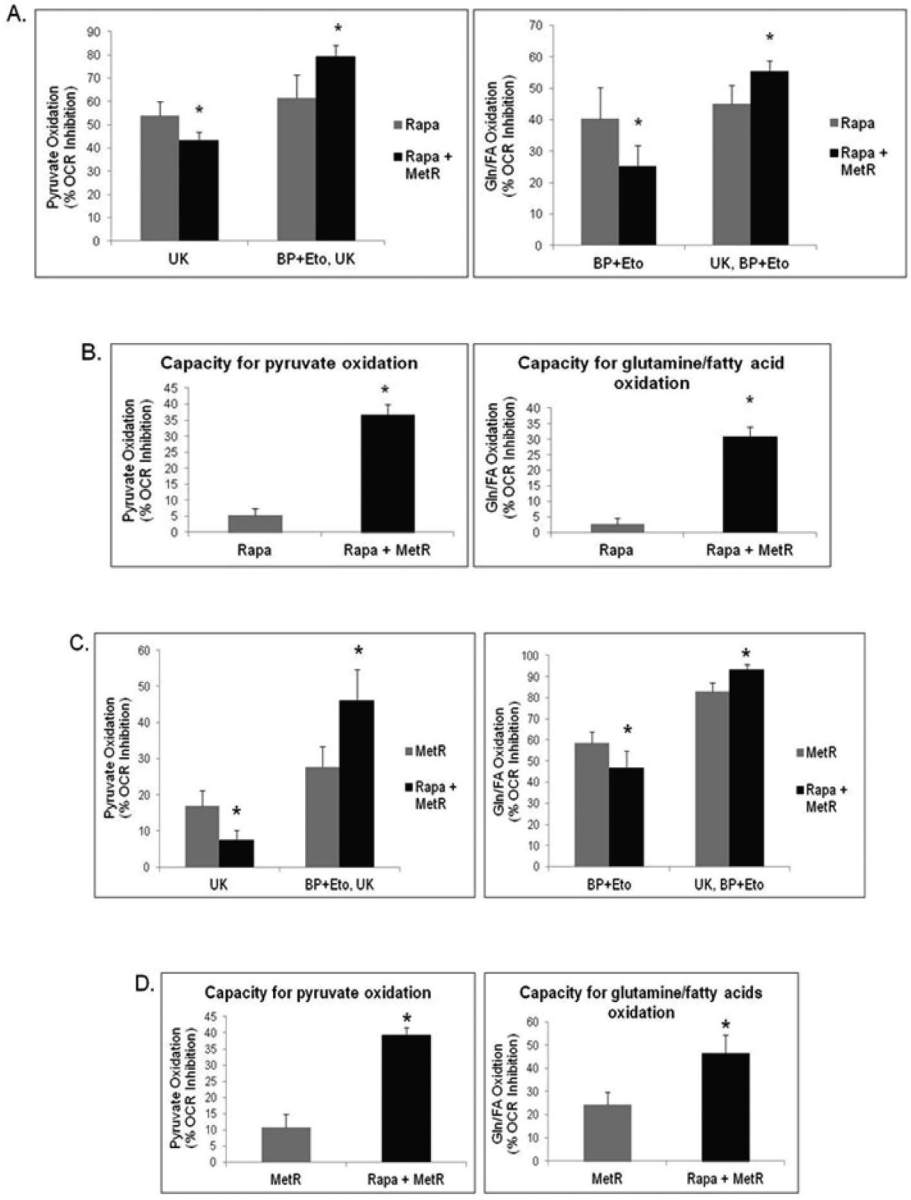

FIGURE 6: The combination of MetR and Rapa increases utilization of alternative carbon sources following inhibition of specific metabolic pathways. Metabolic flexibility, defined as the ability to maintain oxygen consumption following treatment with metabolic pathway pharmacological inhibitor(s), was tested under conditions of Rapa and Rapa plus MetR at 1 mg/l. Panels (A) and (B) contain the results of a comparison of Rapa-treated cultures and cultures treated with the combination of MetR and Rapa. Panels (C) and (D) contain the results of a comparison of methionine-restricted cultures and cultures treated with the combination of MetR and Rapa. Pyruvate oxidation was determined following the addition of UK5099 (inhibitor of mitochondrial pyruvate transporter), while the capacity for pyruvate oxidation was determined following sequential treatment of the glutaminase inhibitor BPTES (10 μM) and Etomoxir (15 μM) followed by UK5099. Glutamine/palmitate oxidation was determined following treatment with BPTES/Etomoxir (left panels in [A] and [C]), while the capacity for glutamine/palmitate oxidation was determined following sequential treatment of UK5099, and the combination of BPTES and Etomoxir (right panels in [A] and [C]). The measurement of spare capacity was based on the difference between capacity and the rate of oxidation for pyruvate oxidation (left panels in [B] and [D]) and glutamine/fatty acid oxidation (right panels in [B] and [D]). OCR and ECAR were normalized to cell number by counting cells in each well at the completion of the assay using flow cytometry. Asterisks represent values that are significantly ($P < 0.05$) different versus control. Significance is based on unpaired, two-tailed, Student's *T* test. Results are representative of two independent experiments.

otherwise. For example, the strong up-regulation of autophagy for proper repurposing of intracellular stores is more pronounced in the Rapa-treated cultures, while the methionine-restricted state produces a need for enhanced recycling of SAM stores as revealed by the increased expression of enzymes related to SAM recycling such as BHMT. This interplay creates a unique metabolic state that appears to prevent transition into senescence. How this relates to chromatin structure and impairment of chromatin remodeling typical of senescence may be explained by the fact that the methyltransferases KMT2D, ASH1L, and SETD1B not only play a role in beta oxidation through carnitine synthesis but also have a role in histone H3 lysine 4 and lysine 36 methylation (Papp and Muller, 2006). The expression level of these specific genes was greater than 10-fold higher when the methionine-restricted, Rapa-treated combination cultures reached very high population doublings (Experimental Point 3), suggesting they were important to the sustained proliferation of these cultures. Consistent with this, trimethylation of H3K4 is one of the strongest hallmarks of open chromatin. In addition, ASH1L has been reported to methylate lysine 36 on histone H3 (Byrd and Shearn, 2003), which is important for transcriptional fidelity during senescence (He *et al.*, 2008; Sen *et al.*, 2015) and potentially antagonizing polycomb silencing (Miyazaki *et al.*, 2013). These methyltransferases are also implicated in histone methylation of telomere regions (Caslini *et al.*, 2009), further supporting an impact on the senescence program. Further, levels of H3 are known to decrease during senescence and the protein is processed during senescence to remove the tail region (Gregory *et al.*, 2007; Ivanov *et al.*, 2013; Duarte *et al.*, 2014). The increase in H3 levels and H3 modifications in general suggests that the senescence-associated changes in H3 are mitigated by the treatment (Figure 8). Since the intracellular concentration of S-adenosyl methionine is in the range of the K_m for the methyltransferases (Mentch *et al.*, 2015; Mentch and Locasale, 2016), shifts in methionine concentrations and methyltransferase levels can potentially affect regional histone modifications. This connection between metabolic enzymes and chromatin remodeling may partially underlie the effect of this unique metabolic state (observed under the combination of MetR plus Rapa treatment) on the global chromatin remodeling associated with the senescence program.

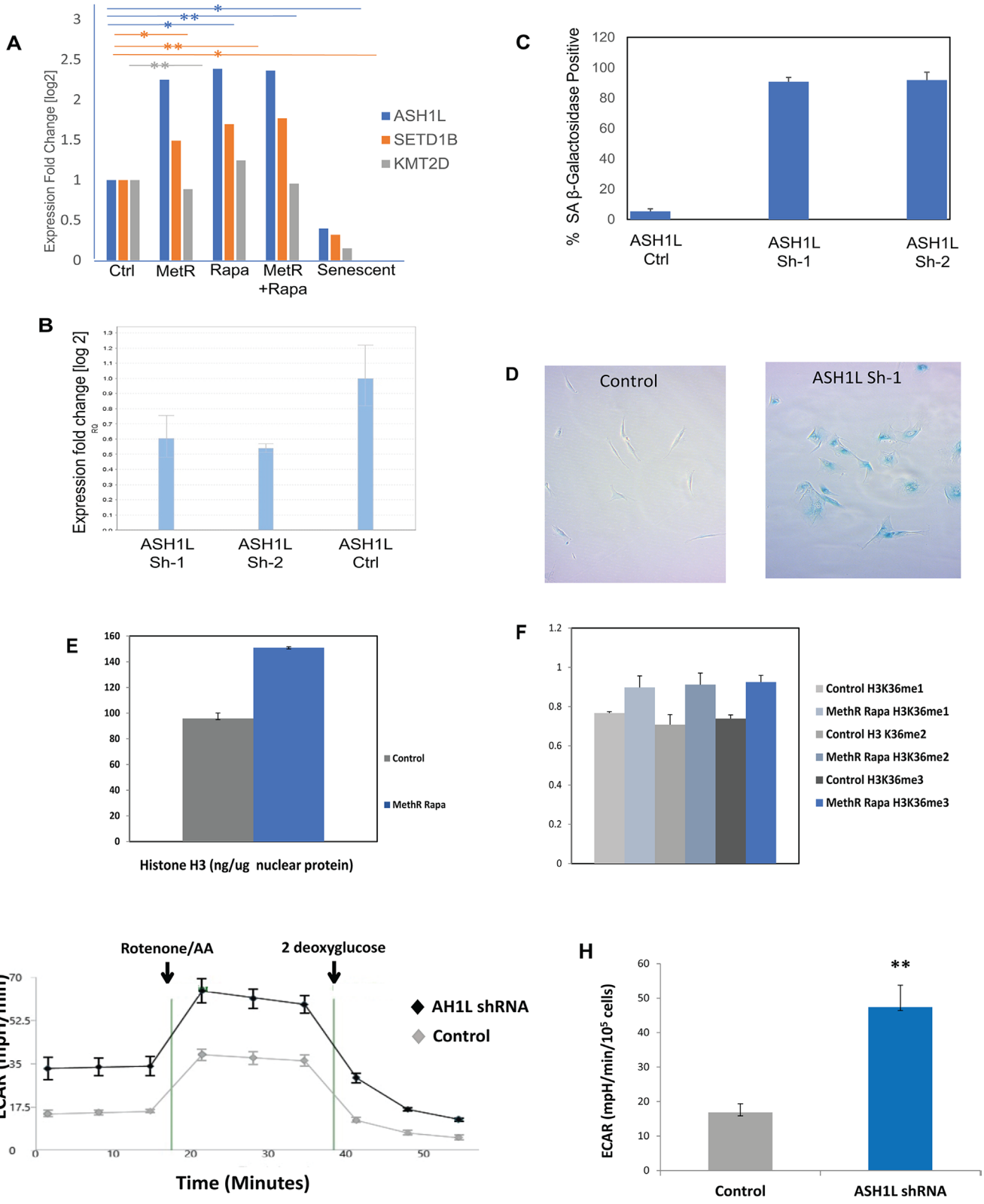

FIGURE 7: Reduced expression of histone methyltransferase ASH1L induces premature senescence while histone H3 levels are maintained by MetR plus Rapa. In Panel (A), quantitative RT-PCR analysis of mRNA levels for the methyltransferases ASH1L, SETD1B, and KMT2D is shown. Values were normalized relative to GAPDH. Bars labeled Ctrl show values from early passage cultures in comparison to early passage cultures under MetR (1 mg/l), Rapa treatment, or the combination of MetR + Rapa or senescent from cultures grown to late passage (>50 population doublings) that have entered senescence. Panel (B) contains quantitative real-time RT-PCR analysis of ASH1L mRNA levels in HCF cells following infection with two independent lentiviral vectors expressing shRNA constructs targeting the ASH1L mRNA. Panel (C) shows the percentage of cells stained positive for SA-β-galactosidase activity in the 2 shRNA-expressing

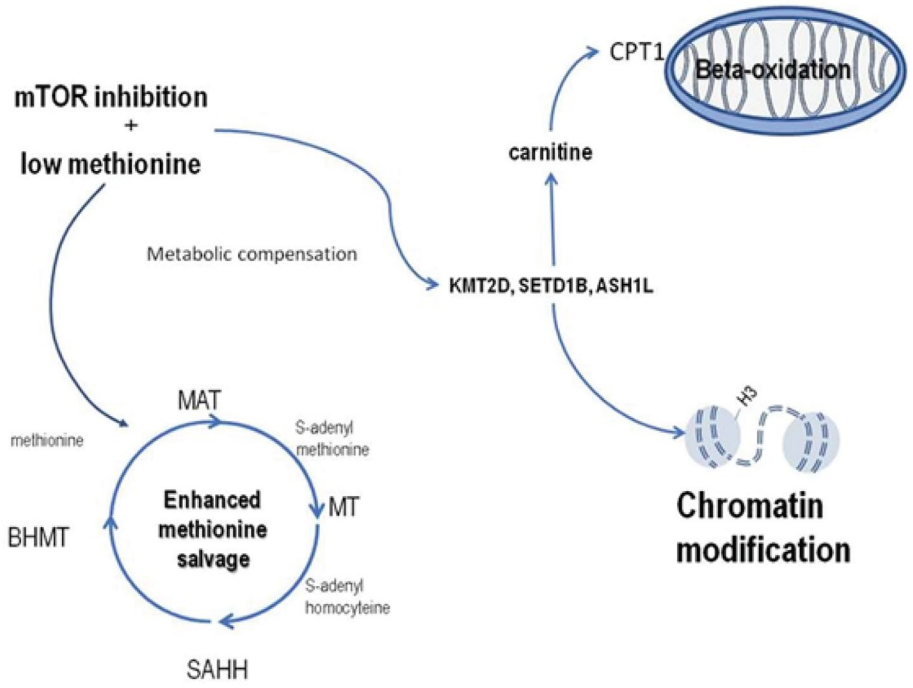

FIGURE 8: Schematic representation of dual roles for the KMT2D, SETD1B, and ASH1L methyltransferases in beta-oxidation and histone modification. The schematic highlights a potential role for the regulation of both metabolic and epigenetic changes during senescence by the three enzymes KMT2D, SETD1B, and ASH1L. Rate limiting steps in both carnitine synthesis and histone 3 methylation at lysine 4, a critical site for transcriptional activation of gene promoters. Targeting the most differentially expressed of these enzymes, ASH1L, results in a dramatic decrease in transcription, a metabolic shift toward glycolysis, and senescence. We propose that these three enzymes help coordinate metabolic status with epigenetic modifications during senescence.

MATERIALS AND METHODS

Request a protocol through *Bio-protocol*.

Cell culture and cell culture reagents

HCF cells were cultivated in MEM supplemented with 10% fetal bovine serum, 1% L-glutamine, 1% MEM vitamins, and 1% MEM nonessential amino acids according to a standard culture protocol for life span analysis of human diploid fibroblasts (Cristofalo and Charpentier, 1980). For MetR studies, cells were cultured in methionine-free DMEM supplemented with 10% fetal bovine serum and 1% L-glutamine. L-methionine was added to a final concentration of 30 mg/l for standard cultures. Methionine-restricted cultures contained either 3 mg/l of methionine (90% reduced) or 1 mg/l of methionine (97% reduced). MetDEF lacked methionine in the culture media (0 mg/l), which is known to be a source of methionine. Parallel sets of cultures were maintained in identical growth medium with the addition of 1 nM Rapa (Enzo Life Sciences). For cell culture under normoxia, cells were cultured for the entirety of the life span in a hypoxic chamber (Coy Laboratory) pre-equilibrated to 6% O_2 and 5% CO_2 at 37°C. For nucleotide supplementation studies, cells were maintained in the standard culture medium as described above with 1, 5, or 10× the standard concentration of nucleotides added to the culture medium. Population doubling was calculated according to Cristofalo and Charpentier (Cristofalo and Charpentier, 1980).

Immunoblotting

Cell protein extracts were prepared by extraction with RIPA buffer containing a protease inhibitor cocktail (Sigma-Aldrich) and protein concentration was quantified using a bicinchoninic acid assay (Pierce Biotechnology). Immunoblot analysis was performed using 15 to 30 µg of protein extracts subjected to SDS–PAGE and transferred onto nitrocellulose membranes (Bio-Rad). Blots were incubated with antibodies specific for the following proteins: beta-actin (A2066)(Sigma-Aldrich); p16 (JC8, sc-56330), and HDM2 (SMP-14, sc-965) (Santa Cruz Biotechnologies); p53 (Ab-6, OP43) and p21 (Ab-1,OP64) (EMD Millipore); phospho (S235/236)-ribosomal protein S6 (2211), ribosomal protein S6 (54D2, 6194), phosphor (S473)-AKT (D9E, 4060S), AKT (C67E7, 4691S), beta-tubulin (10376), eEF2 (2332S), phosphor (T898) GCN2 (3301), GCN2 (3302), phosphor (S51)-eIF2α (9721), eIF2α (9722), ATG5 (2630), ATG12 (2010), and LC3B (2775) (Cell Signaling); p62 (Q13501)(Enzo Life Sciences); IL-6 (A0286) (NeoBiolab); and lamin B1 (ab16048) (Abcam), according to the manufacturers' instructions. Immunoblots were visualized using 800 LI-COR secondary antibodies with IRDye 680 on a LI-COR Odyssey Imaging System analyzed utilizing LI-COR Odyssey Software Version 3.0 (LI-COR Biosciences).

Mitochondrial respiration (oxygen consumption), ECAR, and glucose uptake

Oxygen consumption and the ECAR were measured on a Seahorse XF24 Analyzer (Seahorse Bioscience) using the XF Cell Mito Stress

cultures examined in (B). Panel (D) contains representative photographs of HCF cells stained for SA-β-galactosidase harboring either the pLKO vector or the pLKO expressing one of the two shRNA molecules directed against ASH1L. Induction of senescence was repeated in two independent experiments. Differences marked with a single asterisk represent significance at $P < 0.05$. Differences marked with a double asterisk represent significance at $P < 0.01$. Panel (E) shows the histone H3 content of late passage cells and late passage cells cultured under MetR + Rapa conditions. Panel (F) shows relative levels of H3K36me1, 2, and 3. Relative quantities for the modifications are presented as absorbance units per ng H3 protein. Panel (G) shows the graphic output of the ECAR generated from a Seahorse extracellular flux analysis system. Panel (H) contains an integrated quantification of the ECAR from the Seahorse extracellular flux analysis. The flux analysis results are representative of three independent experiments and two independent lentiviral vectors expressing shRNA constructs targeting the ASH1L mRNA shown in (B). Differences marked with a single asterisk are significant at $P < 0.05$ and differences marked with a double asterisk are significant at $P < 0.01$.

Test and XF Mito Fuel Flex Test kits, respectively. Cells were seeded at a density of 15,000 to 25,000 cells per well in an XF24 microplate. The plates were then loaded into the analyzer, which was preloaded with a sensor cartridge containing oligomycin, carbonilcyanide p-triflouromethoxyphenylhydrazone (FCCP), and rotenone/antimycin A for the Mito Stress Test and UK5099, BPTES, and etomoxir for the Mito Fuel Flex Test. Oxygen consumption was measured after sequential addition of the compounds in a minimum of three independent experiments. Respiration rates and ECARs were assessed according to published methods (Dranka *et al*., 2011; Hill *et al*., 2012). Mitochondrial respiration was calculated based on OCR measurements. All OCR measurements were performed using triplicate samples at a minimum. For the Mito Stress Test, basal respiration represents the initial OCR, while maximal respiration represents oxygen consumption following FCCP addition. ATP-linked respiration represents the oligomycin-sensitive oxygen change to the basal OCR. Nonmitochondrial sources of oxygen consumption were subtracted by normalizing to the rotenone/antimycin A-insensitive OCR measurements. For the Mito Fuel Flex Test, the calculated rate of oxidation was based on the percentage of OCR inhibition after treatment with metabolic pathway pharmacological inhibitor(s). Pyruvate oxidation was determined following treatment with UK5099 (8 μM), while capacity was determined after sequential treatment with BPTES (10 μM)/etomoxir (15 μM) followed by UK5099 treatment. Glutamine/palmitate oxidation was determined following treatment with BPTES/etomoxir, while capacity was determined following sequential treatment with UK5099 followed by BPTES/etomoxir treatment. The spare capacity was determined based on the difference between capacity and oxidation. OCRs and ECARs were normalized to the cell number by counting cells in each well at the completion of the assay using the Guava EasyCyte Mini. Glucose uptake was determined by measuring glucose levels in the media using an ACCU-CHEK glucometer and was normalized to cell numbers using a Guava EasyCyte Mini flow cytometer.

Quantitative real-time PCR and NanoString analysis

RNA was isolated from cells using TRIzol solution (ThermoFisher Scientific) or the RNeasy Kit (Qiagen). RNA was then subjected to quantitative real-time PCR (qRT-PCR) or NanoString analysis. TaqMan Assays (ThermoFisher Scientific) were utilized for qRT-PCR with the following probe sets: GAPDH (Hs99999905-m1), ATF4 (Hs00909569_g1), CHOP (Hs00358796_g1), and RPL5 (Hs03044958_g1). For qRT-PCR analysis, ATF4 and CHOP levels were normalized to GAPDH levels. All qRT-PCR experiments were conducted using a Stratagene Mx3000P thermocycler. NanoString analysis was performed according to the manufacturer's protocol (Geiss *et al*., 2008).

RNA extraction, cDNA synthesis, and sequencing

Total RNA was isolated from triplicate samples of HCFs (early passage, late passage, methionine restricted, Rapa treated, and combination treated) using TRIzol extraction. Total RNA was then submitted to the Drexel University College of Medicine Center for Genomic Sciences for quality control, polyA selection, cDNA library preparation, and sequencing. The cDNA library was prepared using the TruSeq Stranded mRNA Library Prep Kit (Illumina) and sequenced using the Illumina NextSeq 500 platform over two runs with the 75-cycle High Output Kit (Version 1). Two independent sequencing reactions were performed.

Mapping of RNA-Seq reads

For read alignments, the GRCh37.75 reference was used. The following alignment algorithms were used to map all samples to the reference. Specifically, the Burrows-Wheeler Aligner algorithm (BWA, v0.7.10) and the STAR aligner (v2.4.0 h) in conjunction with downstream analysis tools were utilized to independently arrive at a set of differentially expressed genes. Importantly, only uniquely mapping reads were retained by filtering with Sambamba (v0.5.0) using a mapping quality of ≥1 for BWA and 255 for STAR. General mapping statistics were generated using the Sambamba Flagstat tool or the STAR aligner.

Generating count tables

A series of Bioconductor packages for R were used to create count tables reporting the number of reads mapping to each transcript in the reference gene set using either the BWA or the STAR alignments. Specifically, these packages were R Samtools (v1.18.2), Genomic Features (v1.18.3), and Genomic Alignments (v1.2.1). The output of this workflow was a data table with counts per annotated gene per sample suitable for direct use in the differential expression analysis. In addition, the counts per gene were normalized using the reads per kilobase of transcript per million mapped reads (RPKM) method by dividing the total counts aligned to each gene by the kilobase length of that feature and the total number of millions of reads in the sample.

Differential gene expression analysis

While independent differential gene expression analyses were tested, the majority of differential gene expression analysis was performed using the DESeq2 (v1.6.3) package in R. Individual contrasts were conducted within the DESeq2-generated object on raw counts normalized by the median ratio method and statistical significance was determined after multiple testing corrections and calculation of fold changes based on a fitted model of normalized counts. For this analysis, significant differential gene expression was determined using a false discovery rate-adjusted *P* value of 0.05 (adjusted with the Benjamini-Hochberg adjustment). Venn diagrams were generated using R. Additional data visualization was performed using R, including the ggplot2 package (v1.0.0). To follow general convention and to provide estimated expression levels, plotting was performed using RPKM values. However, statistical significance was generated using the normalized median ratio values within DESeq2.

Validation of differential expression analysis

Gene read counts from replicates within a group correlated with adjusted R-squared values >0.98 when plotted against one another. To confirm there was no sequencing bias between RNA sequencing preps and runs, we ran one RNA sample (EarlyPassA) through both runs. When gene read counts were plotted against one another, the adjusted R-squared value was 0.994, suggesting that these two samples were extremely similar despite being handled separately (Supplemental Figure S8). As an additional validation, mRNA expression values from the RNA-Seq data were compared with results acquired previously using NanoString analysis, which provides direct fluorescent-labeled mRNA counts using two contiguous probes for each mRNA species. The expression of 44 genes from both mRNA counting methods, when plotted against each other for each of the five conditions, confirmed that these two methods did indeed corroborate the findings of R-squared values, ranging from 0.37 to 0.53 for each treatment comparison (*P* values 5.5×10^{-6} to 1.6×10^{-8}; Supplemental Figure S9).

Pathway analysis and gene ontology

DAVID pathway analysis was used for pathway enrichment and gene ontology analysis. Gene lists created through DESeq2 thresholding

were fed into the DAVID functional annotation tool in order to provide Kyoto Encyclopedia of Genes and Genomes (KEGG) pathway correlations and rank important genes involved in the given pathway.

Chromatin accessibility assay

ATAC-seq was performed as described previously (Buenrostro *et al*., 2013), with minor modifications. Nuclei were isolated from 50,000 cell pellets from biological duplicates for each condition. Cell pellets were washed with 50 µl of cold 1× phosphate-buffered saline (VWR LifeScience) and centrifuged at 500 × *g* for 5 min. Cells were lysed using 50 µl cold lysis buffer (10 mM Tris-Cl, Invitrogen), pH 7.4, 10 mM NaCl (Lonza), 3 mM $MgCl_2$ (Invitrogen), and 0.1% vol/vol NP-40 (US Biological). The nuclei were centrifuged at 500 × *g* for 10 min at 4°C. Nuclei pellets were resuspended in 25 µl transposase reaction mix (25 µl 2× TD buffer, 2.5 µl transposase (Illumina) and 22.5 µl of nuclease-free water). The transposition reaction was carried out for 30 min at 37°C. Tagmented DNA was purified with a MinElute Reaction Cleanup kit (Qiagen), according to the manufacturer's instructions; 20 µl of tagmented DNA was used to amplify library fragments in a 50 µl PCR reaction. The PCR reaction included 5 µl of both index primers (i5 and i7) (Illumina), 15 µl Nextera PCR Master Mix, and 5 µl PCR Primer Cocktail. Amplification was performed using the following PCR conditions: 72°C for 3 min, 98°C for 30 s, followed by thermocycling at 98°C for 10 s, 63°C for 30 s, and 72°C for 1 min. To reduce GC and size bias in the PCR reaction, the reaction was monitored using quantitative PCR (qPCR) to stop amplification prior to saturation. To do this, the libraries were amplified for 5 cycles. After 5 cycles, 10 µl of the PCR was taken for further amplification using PCR index primers i5 and i7. This reaction was run for 20 cycles to determine the additional number of cycles needed for the remaining 45 µl reaction. Libraries were amplified for a total of 10–12 cycles. Final library purification was performed using AMPure XP beads with a size selection to enrich for fragments shorter than 700 bp and to remove primer dimers and large >1000 bp fragments. Library concentration and fragment size distribution were assessed by Bioanalyzer High Sensitivity DNA kit (Agilent). Libraries were sequenced on an Illumina HiSeq2500 using V4 chemistry in order to produce 75 bp pair-end reads. Unless specified otherwise, sequencing raw data was processed as follows using a customized version of DNAnexus software (DNAnexus Inc.; https://dnanexus.com) and CHIPseeker package in R/Bioconductor. Initial quality control analysis was performed using FastQC (https://www.bioinformatics.babraham.ac.uk/projects/fastqc/). Additional QC was generated with DNAnexus software. All replicates for all samples were cleared for current ENCODE QC standards before proceeding for further analysis. After sequencing, reads were demultiplexed using the provided barcodes, the Illumina index read and the tool "Illumina Demultiplex." The reads were processed and mapped using DNAnexus. For each obtained sample, adaptors were trimmed. The trimmed reads were aligned to GRCh38 human reference genome using Bowtie2. Mapped reads were filtered for mapping quality and proper pairing using SAMtools. Duplicate fragment reads and reads mapping to the mitochondrial genome were excluded from all downstream analysis using Picard Mark Duplicate. Filtered reads were sorted and indexed using SAMtools. Peaks were called on each sample using MACS2 in DNAnexus. Narrow peaks (*P*-value threshold = 0.01) generated were filtered for blacklist regions (regions with a very high ratio of multimapping to unique mapping reads and high variance in mappability. This includes repeat elements such as satellite DNA, and centromeric and telomeric repeats). Both alignment and peak calling were performed on both replicates in each sample by creating pseudoreplicates. Peak annotation was performed using the CHIPseeker package in R/Bioconductor. Validation of transcription start sites, insert size analysis, and chromatin accessibility plots for each chromosome are presented in Supplemental File 2.

Telomere length assessment and telomerase activity assay

Telomere length assays were performed by the Risques laboratory at the University of Washington by qPCR (Cawthon, 2002). The service is available as a fee-based service and includes internal quality controls validated by the facility. Telomerase activity was evaluated using the Trapeze assay (EMD Millipore) which utilizes the telomeric repeat amplification protocol(Herbert *et al*., 2006) following manufacturer's instructions.

Histone H3 measurements

Total histone H3 and modified levels of histone H3 were examined using an ELISA-based system produced by Epigentek. Briefly, chromatin-associated proteins were extracted by acid extraction using a histone extraction kit (Epigentek) and evaluated by ELISA using antibodies directed against the total H3 protein and a panel of histone modifications including H3K4, H3K9, H3K36 mono-, di-, and trimethylation. This analysis was performed twice with similar results.

Statistical analysis

The results are representative of at least two independent experiments. A detailed description of the number of repetitions for each set of experiments is provided in the figure legends. Logistic regression for growth curves was performed using Prism Graph Pad. Statistical significance was determined for direct comparisons in RT-PCR, immunoblot analysis, puncta for LC3 and γH2AX foci, and differences in metabolic measurements (ECAR, OCAR, glucose uptake, etc.) using an unpaired two-tailed Student's *t* test. Data sets were subjected to normality tests to verify normal distribution of data. One-way ANOVA with Bonferroni post-hoc analysis was performed on multiple comparison groups where appropriate.

ACKNOWLEDGMENTS

This work was supported by the Commonwealth of Pennsylvania Universal Research Enhancement Formula Grant Program (C.S.), and a fellowship from the Drexel University College of Medicine Aging Initiative (A.A.). The authors thank Sergey Balashov for assistance with RNA sequencing, Lean Dudash for technical assistance, and Leslie Sell for editorial assistance.

REFERENCES

Alvers AL, Wood MS, Hu D, Kaywell AC, Dunn WA Jr, Aris JP (2009). Autophagy is required for extension of yeast chronological life span by rapamycin. Autophagy 5, 847–849.

Berger SL, Sassone-Corsi P (2016). Metabolic signaling to chromatin. Cold Spring Harb Perspect Biol 8, a019463.

Bittles AH, Harper N (1984). Increased glycolysis in ageing cultured human diploid fibroblasts. Biosci Rep 4, 751–756.

Bitto A, Lerner C, Torres C, Roell M, Malaguti M, Perez V, Lorenzini A, Hrelia S, Ikeno Y, Matzko ME, *et al*. (2010). Long-term IGF-I exposure decreases autophagy and cell viability. PLoS One 5, e12592.

Bjedov I, Toivonen JM, Kerr F, Slack C, Jacobson J, Foley A, Partridge L (2010). Mechanisms of life span extension by rapamycin in the fruit fly Drosophila melanogaster. Cell metabolism 11, 35–46.

Bonnefont JP, Djouadi F, Prip-Buus C, Gobin S, Munnich A, Bastin J (2004). Carnitine palmitoyltransferases 1 and 2: biochemical, molecular and medical aspects. Mol Aspects Med 25, 495–520.

Britton CH, Schultz RA, Zhang B, Esser V, Foster DW, McGarry JD (1995). Human liver mitochondrial carnitine palmitoyltransferase I: characterization of its cDNA and chromosomal localization and partial analysis of the gene. Proc Nat Acad Sci USA 92, 1984–1988.

Buenrostro JD, Giresi PG, Zaba LC, Chang HY, Greenleaf WJ (2013). Transposition of native chromatin for fast and sensitive epigenomic profiling

of open chromatin, DNA-binding proteins and nucleosome position. Nat Methods 10, 1213–1218.
Byrd KN, Shearn A (2003). ASH1, a Drosophila trithorax group protein, is required for methylation of lysine 4 residues on histone H3. Proc Nat Acad Sci USA 100, 11535–11540.
Campisi J (2013). Aging, cellular senescence, and cancer. Annu Rev Physiol 75, 685–705.
Caslini C, Connelly JA, Serna A, Broccoli D, Hess JL (2009). MLL associates with telomeres and regulates telomeric repeat-containing RNA transcription. Molecular and cellular biology 29, 4519–4526.
Cawthon RM (2002). Telomere measurement by quantitative PCR. Nucleic Acids Res 30, e47.
Coppe JP, Desprez PY, Krtolica A, Campisi J (2010). The senescence-associated secretory phenotype: the dark side of tumor suppression. Annu Rev Pathol 5, 99–118.
Coppe JP, Patil CK, Rodier F, Sun Y, Munoz DP, Goldstein J, Nelson PS, Desprez PY, Campisi J (2008). Senescence-associated secretory phenotypes reveal cell-nonautonomous functions of oncogenic RAS and the p53 tumor suppressor. PLoS Biol 6, 2853–2868.
Cristofalo VJ, Charpentier R (1980). A standard procedure for cultivating human diploid fibroblast like cells to study cellular aging. J Tissue Culture Methods 6, 117–121.
De Cecco M, Criscione SW, Peckham EJ, Hillenmeyer S, Hamm EA, Manivannan J, Peterson AL, Kreiling JA, Neretti N, Sedivy JM (2013). Genomes of replicatively senescent cells undergo global epigenetic changes leading to gene silencing and activation of transposable elements. Aging Cell 12, 247–256.
Dranka BP, Benavides GA, Diers AR, Giordano S, Zelickson BR, Reily C, Zou L, Chatham JC, Hill BG, Zhang J, *et al.* (2011). Assessing bioenergetic function in response to oxidative stress by metabolic profiling. Free Radic Biol Med 51, 1621–1635.
Dreesen O, Chojnowski A, Ong PF, Zhao TY, Common JE, Lunny D, Lane EB, Lee SJ, Vardy LA, Stewart CL, Colman A (2013). Lamin B1 fluctuations have differential effects on cellular proliferation and senescence. J Cell Biol 200, 605–617.
Duarte LF, Young AR, Wang Z, Wu HA, Panda T, Kou Y, Kapoor A, Hasson D, Mills NR, Ma'ayan A, *et al.* (2014). Histone H3.3 and its proteolytically processed form drive a cellular senescence programme. Nat Commun 5, 5210.
Geiss GK, Bumgarner RE, Birditt B, Dahl T, Dowidar N, Dunaway DL, Fell HP, Ferree S, George RD, Grogan T, *et al.* (2008). Direct multiplexed measurement of gene expression with color-coded probe pairs. Nat Biotechnol 26, 317–325.
Gregory GD, Vakoc CR, Rozovskaia T, Zheng X, Patel S, Nakamura T, Canaani E, Blobel GA (2007). Mammalian ASH1L is a histone methyltransferase that occupies the transcribed region of active genes. Mol Cell Biol 27, 8466–8479.
Hansen M, Chandra A, Mitic LL, Onken B, Driscoll M, Kenyon C (2008). A role for autophagy in the extension of life span by dietary restriction in C. elegans. PLoS Genet 4, e24.
Hayflick L (1965). The limited *in vitro* lifetime of human diploid strains. Exp Cell Res 37, 614–636.
He J, Kallin EM, Tsukada Y, Zhang Y (2008). The H3K36 demethylase Jhdm1b/Kdm2b regulates cell proliferation and senescence through p15(Ink4b). Nat Struct Mol Biol 15, 1169–1175.
Herbert BS, Hochreiter AE, Wright WE, Shay JW (2006). Nonradioactive detection of telomerase activity using the telomeric repeat amplification protocol. Nat Protoc 1, 1583–1590.
Hill BG, Benavides GA, Lancaster JR Jr, Ballinger S, Dell'Italia L, Jianhua Z, Darley-Usmar VM (2012). Integration of cellular bioenergetics with mitochondrial quality control and autophagy. Biol Chem 393, 1485–1512.
Ivanov A, Pawlikowski J, Manoharan I, van Tuyn J, Nelson DM, Rai TS, Shah PP, Hewitt G, Korolchuk VI, Passos JF, *et al.* (2013). Lysosome-mediated processing of chromatin in senescence. J Cell Biol 202, 129–143.
James EL, Michalek RD, Pitiyage GN, de Castro AM, Vignola KS, Jones J, Mohney RP, Karoly ED, Prime SS, Parkinson EK (2015). Senescent human fibroblasts show increased glycolysis and redox homeostasis with extracellular metabolomes that overlap with those of irreparable DNA damage, aging, and disease. J Proteome Res 14, 1854–1871.
Johnson JE, Johnson FB (2014). Methionine restriction activates the retrograde response and confers both stress tolerance and life span extension to yeast, mouse and human cells. PLoS One 9, e97729.
Kabil H, Kabil O, Banerjee R, Harshman LG, Pletcher SD (2011). Increased transsulfuration mediates longevity and dietary restriction in Drosophila. Proc Nat Acad Sci USA 108, 16831–16836.
Koziel R, Ruckenstuhl C, Albertini E, Neuhaus M, Netzberger C, Bust M, Madeo F, Wiesner RJ, Jansen-Durr P (2014). Methionine restriction slows down senescence in human diploid fibroblasts. Aging Cell 13, 1038–1048.
Lerner C, Bitto A, Pulliam D, Nacarelli T, Konigsberg M, Van Remmen H, Torres C, Sell C (2013). Reduced mammalian target of rapamycin activity facilitates mitochondrial retrograde signaling and increases life span in normal human fibroblasts. Aging Cell 12, 966–977.
Liu H, Zhang W, Wang K, Wang X, Yin F, Li C, Wang C, Zhao B, Zhong C, Zhang J, *et al.* (2015). Methionine and cystine double deprivation stress suppresses glioma proliferation via inducing ROS/autophagy. Toxicol Lett 232, 349–355.
Mentch SJ, Locasale JW (2016). One-carbon metabolism and epigenetics: understanding the specificity. Ann NY Acad Sci 1363, 91–98.
Mentch SJ, Mehrmohamadi M, Huang L, Liu X, Gupta D, Mattocks D, Gomez Padilla P, Ables G, Bamman MM, Thalacker-Mercer AE, *et al.* (2015). Histone methylation dynamics and gene regulation occur through the sensing of one-carbon metabolism. Cell Metab 22, 861–873.
Miyazaki H, Higashimoto K, Yada Y, Endo TA, Sharif J, Komori T, Matsuda M, Koseki Y, Nakayama M, Soejima H, *et al.* (2013). Ash1l methylates Lys36 of histone H3 independently of transcriptional elongation to counteract polycomb silencing. PLoS Genet 9, e1003897.
Nacarelli T, Azar A, Altinok O, Orynbayeva Z, Sell C (2018). Rapamycin increases oxidative metabolism and enhances metabolic flexibility in human cardiac fibroblasts. Geroscience 40, 243–256
Nacarelli T, Azar A, Sell C (2015). Aberrant mTOR activation in senescence and aging: A mitochondrial stress response? Exp Gerontol 68, 66–70.
Nacarelli T, Sell C (2016). Targeting metabolism in cellular senescence, a role for intervention. Mol Cel Endocrinol 455, 83–92
Pajares MA, Perez-Sala D (2006). Betaine homocysteine S-methyltransferase: just a regulator of homocysteine metabolism? Cellular and molecular life sciences: CMLS 63, 2792–2803.
Papp B, Muller J (2006). Histone trimethylation and the maintenance of transcriptional ON and OFF states by trxG and PcG proteins. Genes Dev 20, 2041–2054.
Parry AJ, Narita M (2016). Old cells, new tricks: chromatin structure in senescence. Mamm Genome 27, 320–331.
Rog-Zielinska EA, Norris RA, Kohl P, Markwald R (2016). The Living Scar–Cardiac Fibroblasts and the Injured Heart. Trends Mol Med 22, 99–114.
Ruckenstuhl C, Netzberger C, Entfellner I, Carmona-Gutierrez D, Kickenweiz T, Stekovic S, Gleixner C, Schmid C, Klug L, Sorgo AG, *et al.* (2014). Life span extension by methionine restriction requires autophagy-dependent vacuolar acidification. PLoS Genet 10, e1004347.
Sen P, Dang W, Donahue G, Dai J, Dorsey J, Cao X, Liu W, Cao K, Perry R, Lee JY, *et al.* (2015). H3K36 methylation promotes longevity by enhancing transcriptional fidelity. Genes Dev 29, 1362–1376.
Shah PP, Donahue G, Otte GL, Capell BC, Nelson DM, Cao K, Aggarwala V, Cruickshanks HA, Rai TS, McBryan T, *et al.* (2013). Lamin B1 depletion in senescent cells triggers large-scale changes in gene expression and the chromatin landscape. Genes Dev 27, 1787–1799.
Shimi T, Butin-Israeli V, Adam SA, Hamanaka RB, Goldman AE, Lucas CA, Shumaker DK, Kosak ST, Chandel NS, Goldman RD (2011). The role of nuclear lamin B1 in cell proliferation and senescence. Genes Dev 25, 2579–2593.
Souders CA, Bowers SL, Baudino TA (2009). Cardiac fibroblast: the renaissance cell. Circ Res 105, 1164–1176.
Strijbis K, Vaz FM, Distel B (2010). Enzymology of the carnitine biosynthesis pathway. IUBMB Life 62, 357–362.
Travers JG, Kamal FA, Robbins J, Yutzey KE, Blaxall BC (2016). Cardiac Fibrosis: The Fibroblast Awakens. Circ Res 118, 1021–1040.
Wang R, Yu Z, Sunchu B, Shoaf J, Dang I, Zhao S, Caples K, Bradley L, Beaver LM, Ho E, *et al.* (2017). Rapamycin inhibits the secretory phenotype of senescent cells by a Nrf2-independent mechanism. Aging Cell 16, 564-574.
Wiley CD, Campisi J (2016). From Ancient Pathways to Aging Cells-Connecting Metabolism and Cellular Senescence. Cell Metab 23, 1013–1021.
Yano S, Li S, Han Q, Tan Y, Bouvet M, Fujiwara T, Hoffman RM (2014). Selective methioninase-induced trap of cancer cells in S/G2 phase visualized by FUCCI imaging confers chemosensitivity. Oncotarget 5, 8729–8736.
Yano S, Takehara K, Zhao M, Tan Y, Han Q, Li S, Bouvet M, Fujiwara T, Hoffman RM (2016). Tumor-specific cell-cycle decoy by Salmonella typhimurium A1-R combined with tumor-selective cell-cycle trap by methioninase overcome tumor intrinsic chemoresistance as visualized by FUCCI imaging. Cell Cycle 15, 1715–1723.
Yecies JL, Manning BD (2011). mTOR links oncogenic signaling to tumor cell metabolism. J Mol Med (Berl) 89, 221–228.